Box-Behnken Design for Photocatalytic Degradation of Sudan Black B by Catalyst-Embedded Multiwalled Carbon Nanotubes

V. S. Angulakshmi[1], S. Mageswari[2*], S. Kalaiselvan[3], R. Padmavathi[3] and K. Parvathi[4]

[1]Department of Chemistry, PSGR Krishnammal College for Women, Coimbatore, TN, India
[2]Department of Chemistry, Vivekanandha College of Engineering for Women, Namakkal, TN, India
[3]Department of Chemistry, M. Kumarasamy College of Engineering, Karur, TN, India
[4]Department of Chemistry, LRG Government Arts College for Women, Tirupur, TN, India
*mmahes15@gmail.com

ABSTRACT

This research employs a Box Behnken design-based technique for photocatalytic use of Multiwalled Carbon Nanotubes (MWCNTs) derived from spray pyrolysis. This procedure was used for photocatalytic degradation applications on Sudan black dye using *Citrus limonum* oil as a carbon precursor and Fe/Co/Mo supported on silica as a catalyst. The influence of initial dye concentration was compared to the effects of H_2O_2, catalyst concentration and solar light intensity. The Response Surface Methodology was used to optimize growth parameters for higher yield and graphitization. The as-grown CNTs were exemplified using scanning and transmission electron microscopy and Raman spectroscopy. This work resulted in the identification of the optimal set of spray pyrolysis turning parameters for achieving high CNT yield and effective decolorization of Sudan black B dye by employing MWCNTs as catalyst. The degree of decolorization of Sudan black B dye increases upto a certain level with an increase in initial H_2O_2 concentration and subsequently declines as excess H_2O_2 hydroxyl radicals formed serve as scavengers, resulting in less dye decolonization.

Keywords: MWCNTs; RSM; Optimization; Dye degradation; CVD; Spray pyrolysis; *Citrus limonum* oil; SEM; HRTEM;

1. INTRODUCTION

Since the 1990s, a great number of international researchers have published extensively on this topic, and it is obvious that the single-walled carbon nanotube is a key component of the prospect of materials science (Coville *et al.* 2011). Carbon nanotubes are circular barrel-shaped allotropic variety of carbon that are typically formed through chemical vapour deposition. These incredible structures have fascinating mechanic, electronic and magnetic properties (Aqel *et al.* 2012). Graphene and carbon nanotubes are given special consideration since they play a critical part in current breakthroughs based on nanomaterials, such as conductive and high-strength composites (Lee *et al.* 2016), simulated implants (Chua *et al.* 2013), drug delivery systems (Ketabi *et al.* 2017), sensors (Arunachalam *et al.* 2018), energy conversion and storage devices (Kumar *et al.* 2018) and field emission displays (Sun *et al.* 2017), nanometer-sized semiconductor devices (Xu *et al.* 2017), hydrogen storage media (Zhao *et al.* 2017) probes (Choi *et al.* 2016) and interconnects (Chen *et al.* 2016). Carbon nanotubes could be produced via chemical vapor deposition (CVD) or plasma-enhanced CVD (PECVD). (Yanase *et al.* 2019), plasma or arc discharge evaporation (Journet *et al.* 1997), laser ablation (Gupta *et al.* 2019)

and thermal synthesis (Moise *et al.* 2019).

All of these processes entail adding energy to the carbon supply producing components that can be reassembled to form groups or single carbon atoms to create CNT. Arc discharge electricity, heat from the CVD furnace (around 900°C), or high-intensity laser light could be used as energy sources (Donaldson *et al.* 2006). Spray pyrolysis is similar to CVD in that it is a single step process, whereas CVD is a two step process (Ghosh *et al.* 2008). Catalysts such as Fe, Co, or Ni were extensively utilized in the synthesis of single-walled and multi-walled CNTs. To enhance the catalytic activity, synergistic impact of the metals utilized in the catalyst was observed (Rakesh *et al.* 2006). Temperature is crucial in the formation of diverse morphologies of nanotubes (Li *et al.* 2002). Camphor, turpentine oil, *Oryzasativa* oil, and *Madhuca longifolia* oil have been employed as carbon precursors in order to produce CNTs (Rakesh *et al.* 2007; Kalaiselvan *et al.* 2018; Mageswari *et al.* 2014; Karthikeyan *et al.* 2014). These natural precursors are inexpensive, renewable, and abundant. Recently, process optimization using design of experiments has gained popularity in allied fields of nanotechnology. The impact of procedure parameters on

carbon nanotube diameter were investigated using RSM (Amirhasan *et al.* 2007). Statistical design of experiments analyzes large data with the fewest number of experiments possible (Goh et al. 2001). Wei-Wen *et al.* (2012) optimized the reaction environment for the production of single-walled carbon nanotubes by means of response surface approach.

Box-Behnken designs were developed to reduce sample size as the number of parameters increased. Box-Behnken is a circular revolving design. It has been used to optimize an extensive choice of chemical and physical processes, and it dictates the number of tests required to be done. The experiments in this study were planned and carried out using a Box-Behnken type response surface design. The Box-Behnken experimental design is used to investigate and optimize the reaction conditions that influence CNT yield and morphology. Carbon nanotubes for wastewater treatment have only recently become the focus of extensive research. Currently, the emphasis is shifting toward multi-walled carbon nanotubes as an alternate for these two-dimensional graphene-based materials (Hayati *et al.* 2020). Moreover, they aid nanomaterials in increasing their strength and increasing their overall surface area, thereby improving photodegradation capability (Shaban *et al.* 2018). Because of their 3D structure, they share qualities with graphene oxide (GO) such as photosensitizing capacity, huge surface area, and elevated adsorption capacity. They also assist nanomaterials in increasing their

strength and surface area, which improves photodegradation capability. Because of their synergy of increasing surface area and trapping excited electrons to minimize recombination, carbon nanotubes engage an essential role in boosting the photocatalytic activity of inefficient metal oxide systems (Chaudhary *et al.* 2016). Carbon nanotubes (CNTs) are potential adsorbents for the treatment of important heavy metals such as Cd(II), Zn(II), and Pb(II) (César *et al.* 2009; Othman *et al.* 2017), dye degradation (Aarthi *et al.* 2007), and water splitting to generate hydrogen at room temperature (Sankeerthana *et al.* 2019).

2. EXPERIMENTAL METHODS

2.1 Preparation of Mixture of Catalysts

To prepare Fe/Co/Mo supported on silica, the wet impregnation method was adopted. The following steps were taken to prepare a Fe/Co catalyst supported on silica (SiO_2) particles (Fe: Co: Mo: SiO_2=1:0.4:4). Metal salts (Merck), namely $Fe(NO_3)_3.6H_2O$ and $Co(NO_3)_2.6H_2O$ and $(NH_4)_6Mo_7O_{24}$, were dissolved in methanol and thoroughly mixed with a silica methanol suspension (Merck). The solvent was then evaporated from the cake, which was then heated to 90-100°C for 3 hours before being removed from the furnace and ground in an agate mortar. The fine powders were then calcined for one hour at 450°C before being reground and loaded into the reactor.
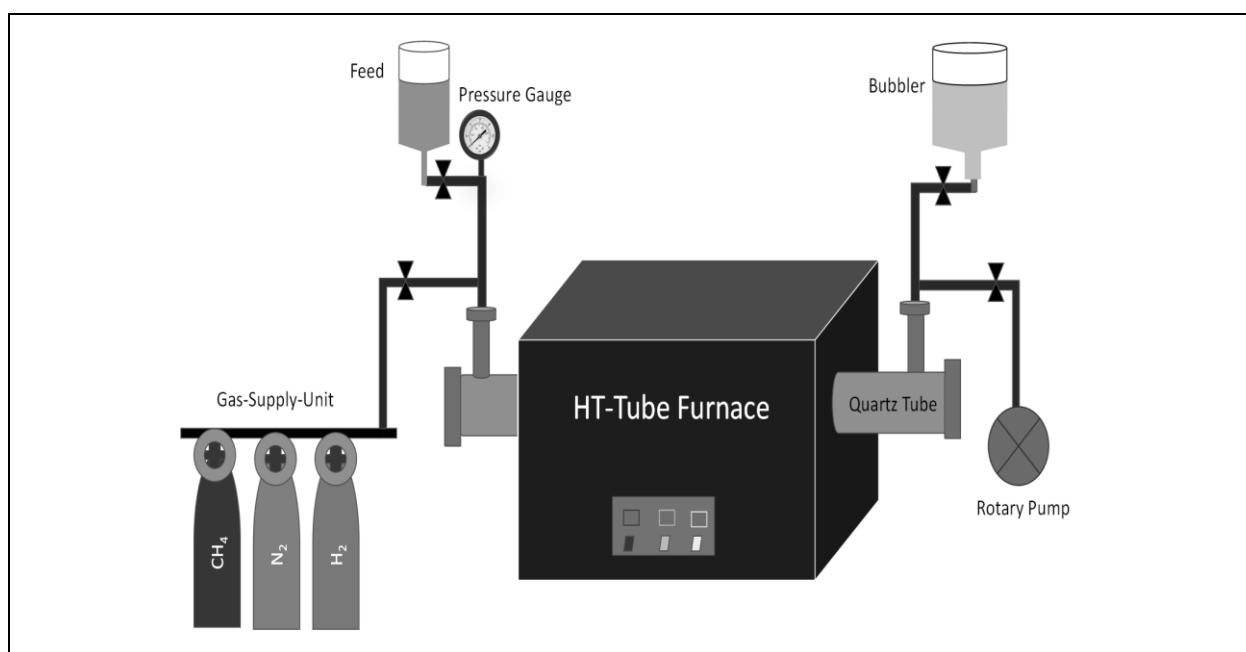

Fig. 1: The diagrammatic arrangement shows the components of the CVD-assisted spray pyrolysis system, including the quartz tube, tube furnace, gas cylinders, rotary pump, pressure gauge, and control panel

Table 1. The experimental choice and stage of the selected precursors input variables

Input Variables	Level (-1)	Level (+1)
A: Temperature (℃)	550	750
B: Catalyst Composition (g)	0.25	0.75
C: Precursor Feed rate (mL)	10	30

2.2 Fabrication and Purification of Nanotubes

Multi-walled carbon nanotubes were synthesized using the CVD assisted spray pyrolysis process (Uthayakumar *et al.* 2022). On the quartz boat, the catalyst was placed. The boat was placed in the furnace for heating. In a typical experiment, the quartz tube was flushed with nitrogen to eliminate air and establish a nitrogen atmosphere before being heated to the reaction temperature. *Citrus limonum* oil precursor solution was sprayed into the quartz tube with nitrogen as a transporter gas. Experiments were carried out by varying the temperature between 550 and 750 ℃ for 45 minutes. The carbon deposit was removed from the reactor and weighed after cooling to room temperature in flowing nitrogen gas. Willems *et al.* (2000) calculated the carbon deposit yield as Carbon deposit% = 100 (m_{Total} - m_{Cat})/m_{Cat}, where the initial quantity of catalyst is denoted by m_{Cat} and m_{Total} is the sample's total mass after the reaction (Hayati *et al.*

2020; Willems *et al.* 2000). The as-grown products were heated for 30 minutes in 1 N HCl at 60℃. Finally, the acid was detached from the samples by washing them with distilled water. The material was dried in air for 2 hours at 120℃. A field-emission scanning electron microscope and a high-resolution transmission electron microscope were used to analyze the surface morphology of as-grown carbon samples. Raman spectroscopy was used to determine the crystalline arrangement of CNT samples.

2.3 Experimental Design

Box-Behnken experimental plan is a three-level design based on a factorial design. To design the trial and randomize the runs, Stat-Ease was utilized in conjunction with Design-Expert Software version 8. Box-Behnken designs empower for the estimation of coefficients in a second-degree polynomial regression as well as the modelling of a quadratic response surface. In the current study, reaction temperature, catalyst composition (Fe-Co-Mo), and precursor feed rate were considered as input variables, while yield percentage was selected as the response variable. Independent variables of highest and lowest levels are displayed in Table 1. Table 2 shows the experimental design matrix for *Citrus limonum* oil by means of the Box-Behnken design, as well as the accompanying experiments. The synthesis of MWNTs was carried out in accordance with the design matrix and the results are listed in Table 2.

Table 2. Box-Behnken design matrix and equivalent response for methyl ester of *Citrus limonum* oil

Run	Factor 1 A: Reaction Temperature(℃)	Factor 2 B: Catalyst Composition (g)	Factor 3 C:Feed rate of Precursor (mL)	Response 1 Yield (%)
1	550	0.5	10	17
2	750	0.75	20	52
3	650	0.75	30	63
4	550	0.5	30	38
5	650	0.5	20	79
6	650	0.75	10	41
7	650	0.5	20	74
8	650	0.5	20	79
9	750	0.5	10	43
10	650	0.5	20	70
,11	650	0.5	20	72
12	550	0.75	20	23
13	550	0.25	20	11
14	750	0.25	20	52
15	650	0.25	10	38
16	650	0.25	30	49
17	750	0.5	30	47

2.4 Photocatalytic Activity Assessment

The photocatalytic experiments were carried out in the presence of natural light. In each experiment, 50 mL of Sudan black B was measured and the absorbance were calculated. Sudan black B had a maximum absorbance of 600 nm. Before irradiation, the photocatalyst suspension (Fe-Co-Mo catalyst-grown MWNTs) was cleaned and blended well in the dark to ensure adsorption equilibrium. The suspension was exposed to sunlight for photodegradation. The suspension sample was collected at 30-minute intervals and centrifuged for 10 minutes at 2500 rpm to remove photocatalyst particles from the suspension. The absorbance was determined at 600 nm. The data were used to compute the percentage of decolorization.

Table 3. ANOVA for RSM variables fitted to a polynomial equation for methyl ester of *Citrus limonum* oil

| Source	Sum of Squares	Df	Mean Square	F-Value	p-value Prob>F
Model	7185.07	9	800.01	24.690	< 0.0001
A-Temperature	1570.00	1	1570.00	49.420	0.0002
B-Catalyst composition	97.00	1	97.00	3.102	0.1300
C-Feed rate of carbon precursor	394.00	1	394.00	13.104	0.0203
AB	6.76	1	6.76	0.192	0.6803
AC	75.02	1	75.02	2.340	0.1850
BC	12.95	1	12.95	0.399	0.5790
A^2	2873.64	1	2873.64	92.883	< 0.0001
B^2	836.19	1	836.19	25.820	0.0012
C^2	776.92	1	776.92	24.960	0.0019
Residual	228.90	7	33.38		
Lack of Fit	196.50	3	67.50	7.850	0.0423
Pure Error	36.20	4	8.70		
Cor Total	7422.85	15			
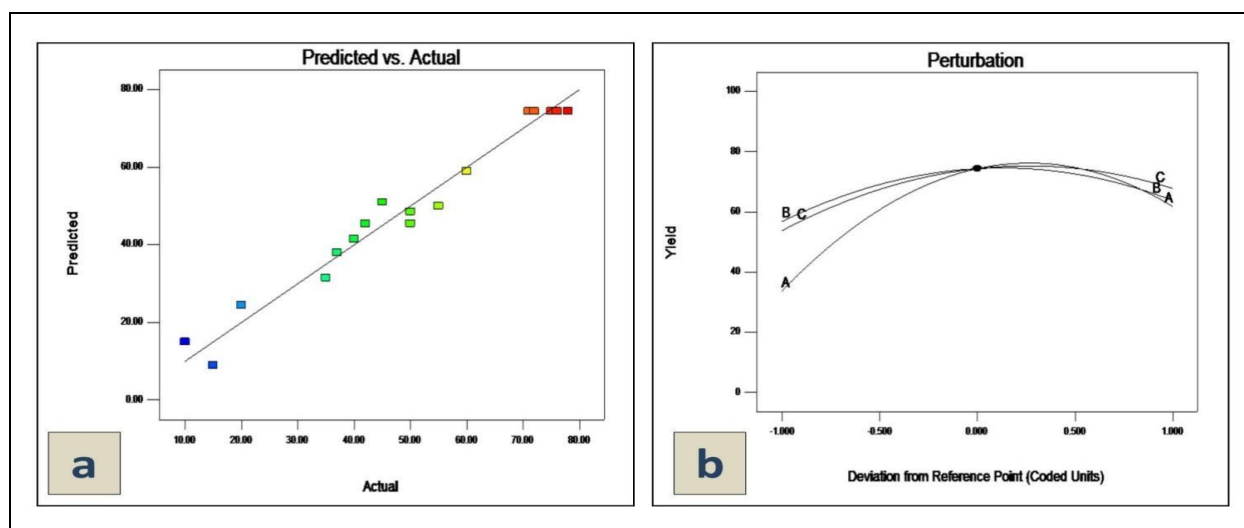
Fig. 2: a) Predicted Vs Actual plot for methyl ester of *Citrus limonum* oil b) Perturbation plot for *Citrus limonum* oil

3. RESULTS AND DISCUSSION

3.1 Box-Behnken Design and Statistics Investigation

The Box-Behnken design move towards examination of the individual and interaction impacts of temperature (°C), catalyst composition (g), and precursor feed rate (mL) on MWNT yield % (as a response). The quadratic model's statistical significance was determined using ANOVA. Table 3 displays the results of the ANOVA for the quadratic equation. According to the ANOVA results, the real correlation involving the response and the significant variables symbolized by the quadratic equations above is correct. The relevance of the coefficient term is found out by the values of F and p; the

greater the F value and the lower the value of p, the more considerable the coefficient term. The model is statistically significant because the p value is less than 0.05. The ANOVA findings for the current synthesis process showed that the Model F value for *Citrus limonum* oil was 24.69, suggesting that there was only a 0.01% chance that a "Model F value" that high might have occurred because of noise. The equation used for regression stated the deviation in the response and that the model was important. *Citrus limonum* oil model terms A, C, A^2, B^2, and C^2 are noteworthy in this study. Other model terms with p values greater than 0.1000 in Table 3 were not significant. The adjusted R^2(Adj-R^2) value is more appropriate for assessing model integrity of a system with varying number of independent variables. The predicted R^2 of 0.5860 for *Citrus limonum* oil values in this model are in rational conformity with the adjusted R^2 values. The results demonstrated that the quadratic model adopted was sufficient for considering the data from the experiment response variables. The perturbation plot can be used to determine which factors have the most influence on the response. A high slope or curvature of a component shows that the reaction is responsive to that variable (Fig 2a).

3.2 Three-Dimensional Response Surface Plots

Three-dimensional surfaces and two-dimensional contours were drawn to explore the interaction of all three factors, with one variable held constant at the middle point and varying the other two variables within the experimental ranges. The contour plot depicts the response across the selection standards in two dimensions. The whole range of two factors can be displayed concurrently. An abrupt slope or curve in a factor in these three-dimensional graphs indicates that the reaction is sensitive to that element. The response surface and contour plots for *Citrus limonum* oil as a function of temperature and catalyst composition are shown in Fig. 2, keeping the precursor feed rate constant at 20 mL. Figure 3 shows that the response in this experiment is temperature dependent. The yield percentage of MWNTs increases with temperature, reaching a maximum for *Citrus limonum* oil at the best temperature (750°C). The low yields reported at 550 and 750°C could be attributed to the catalyst not being activated and accordingly, the high rate of pyrolysis followed by catalyst encapsulation. The FESEM images in Figs. 4a and 4b show the same result. The remarkable yield at 750°C in this study is ascribed to a virtually equal rate of pyrolysis of precursor and the development of CNTs (Shaban *et al*. 2018; Kumar *et al*. 2005).
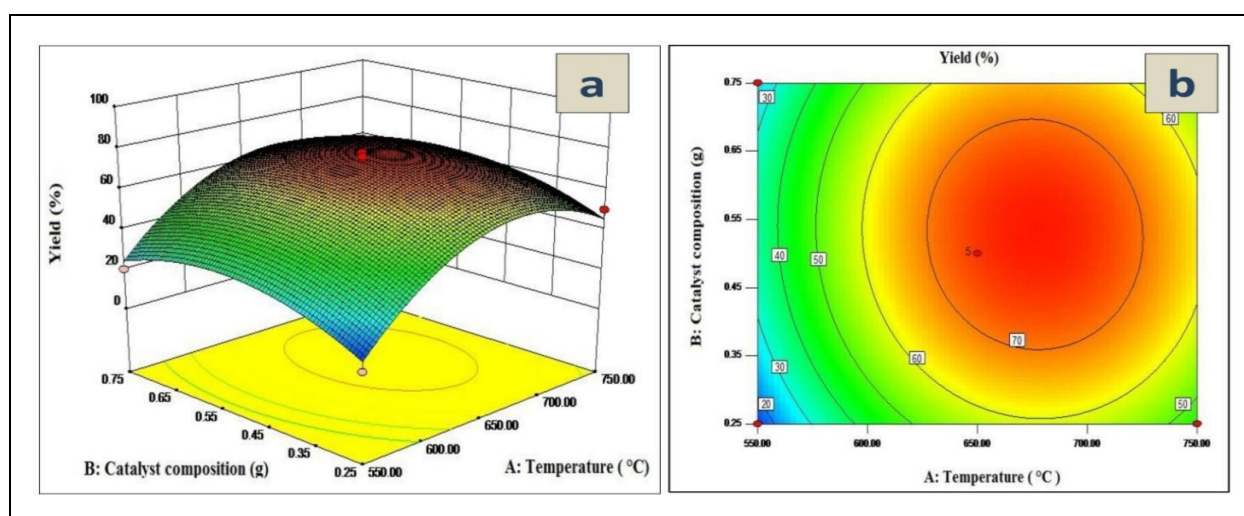

Fig. 3: The response surface and contour plots as the function of temperature and catalyst composition

Figure 5 depicts the combined influence of temperature and carbon precursor feed rate on yield %. The response surface and contour plots for *Citrus limonum* oil were created by controlling the variables (temperature and carbon precursor feed rate) while keeping the catalyst composition (0.5 g) constant. As shown in Fig. 5, increasing the precursor feed rate concentration from 10 mL to 20 mL enhances the MWNT yield %. The end result is in agreement with the HRTEM image (Figs. 6a and 6b). As the flow rate is increased to 30 mL, the yield of MWNTs falls. This is most likely due to catalyst particle deactivation at higher precursor feed rates leading to the production of carbon coated particles, which further limits pyrolysis of the precursor. (Chaudhary *et al*. 2016). Under these experimental conditions, the higher yield of 20 mL per hour acquired for the precursor feed may be due to successful pyrolysis of the precursor.
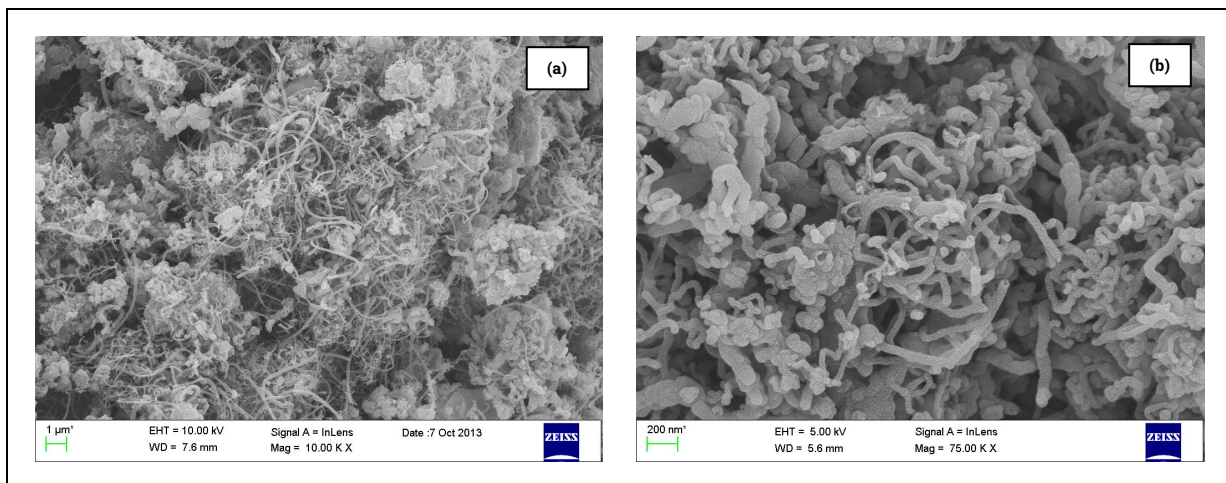
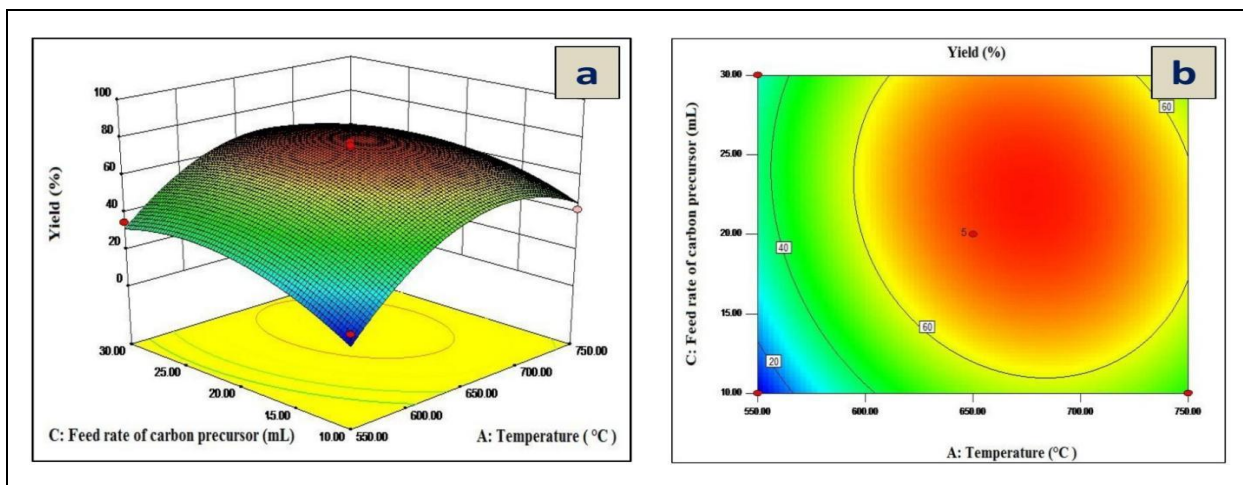**Fig. 4: FESEM image of MWNTs grown at a) 550 °C and b) 750 °C**

Fig. 5: The response surface and contour plots as the function of feed rate (a) and temperature (b) of carbon precursor
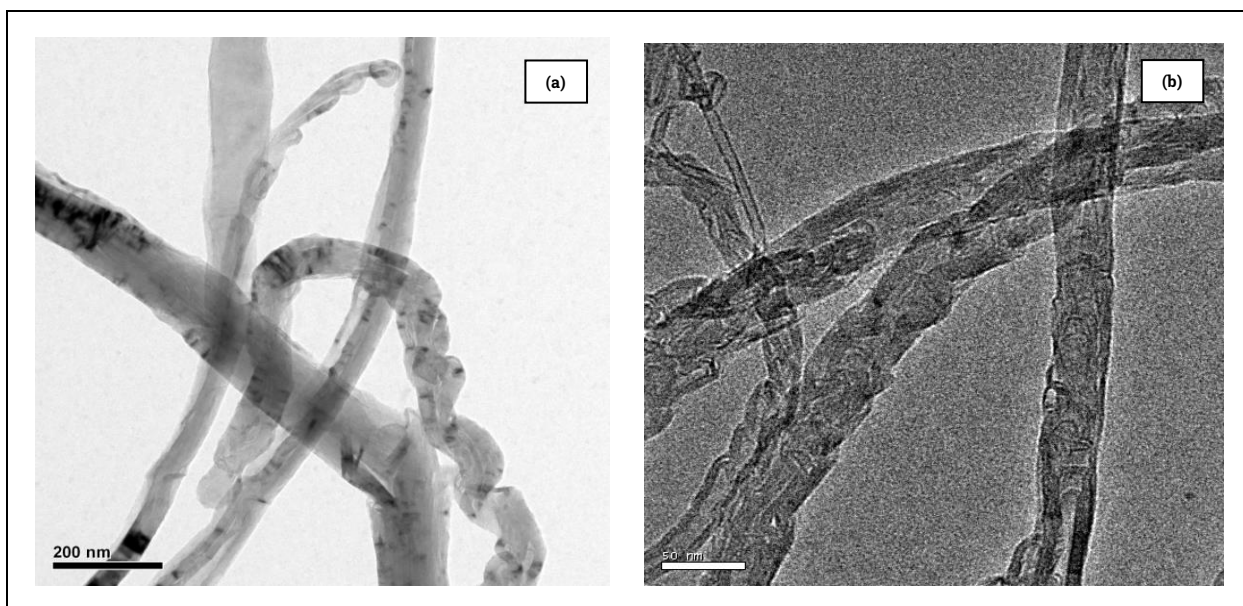

Fig. 6: HRTEM image of MWNTs grown over a) 10 mL and b) 20 mL precursor feed rate

The interactive effect of the carbon precursor feed rate and catalyst composition on the percentage yield of MWNTs at a constant temperature of 750 °C is depicted in Fig. 6. The yield of nanotubes produced over a silica-supported Co catalyst depends on the Co concentration (César et al. 2009; Piedigrosso *et al.* 2000). A substantial link between the catalyst and the yield of MWNTs deposit was identified in this investigation.

Figure 7 depicts how, as the catalyst composition rises, the MWNT yield percentage reaches a maximum and subsequently begins to decline. Increased yield under optimal conditions might be attributed to the synergistic benefits of high catalytic decomposition, CNT growth efficiency, and the promoting characteristics of Fe, Co, and Mo, respectively. The results correlated with the HRTEM images (Figs. 8a and 8b).
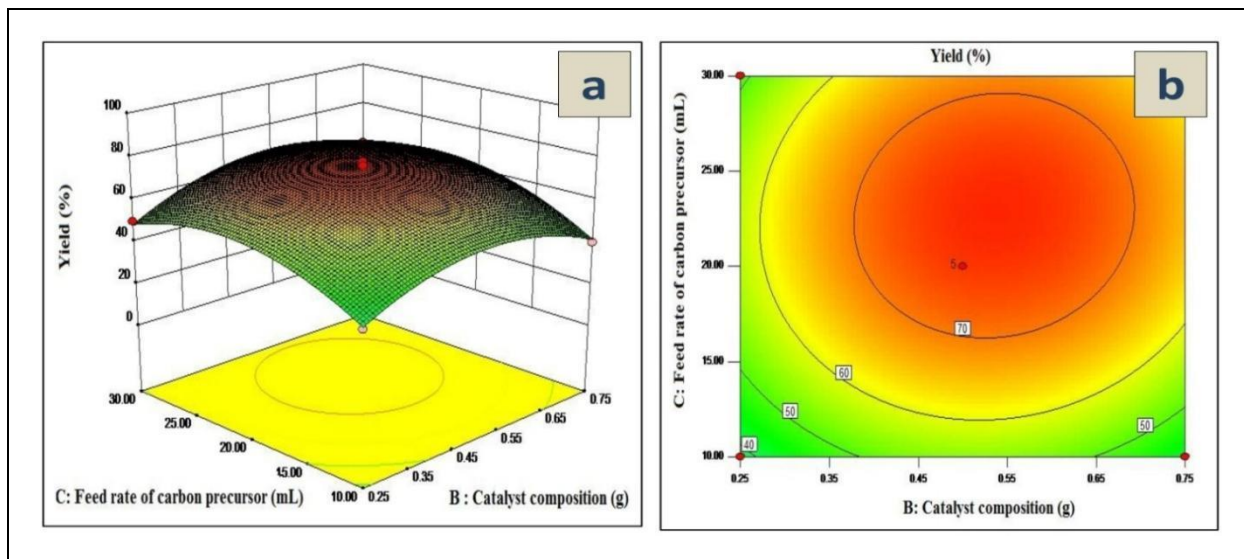

Fig. 7: The response surface and contour plots as an outcome of feed rate (a) and catalyst composition (b) of carbon precursor
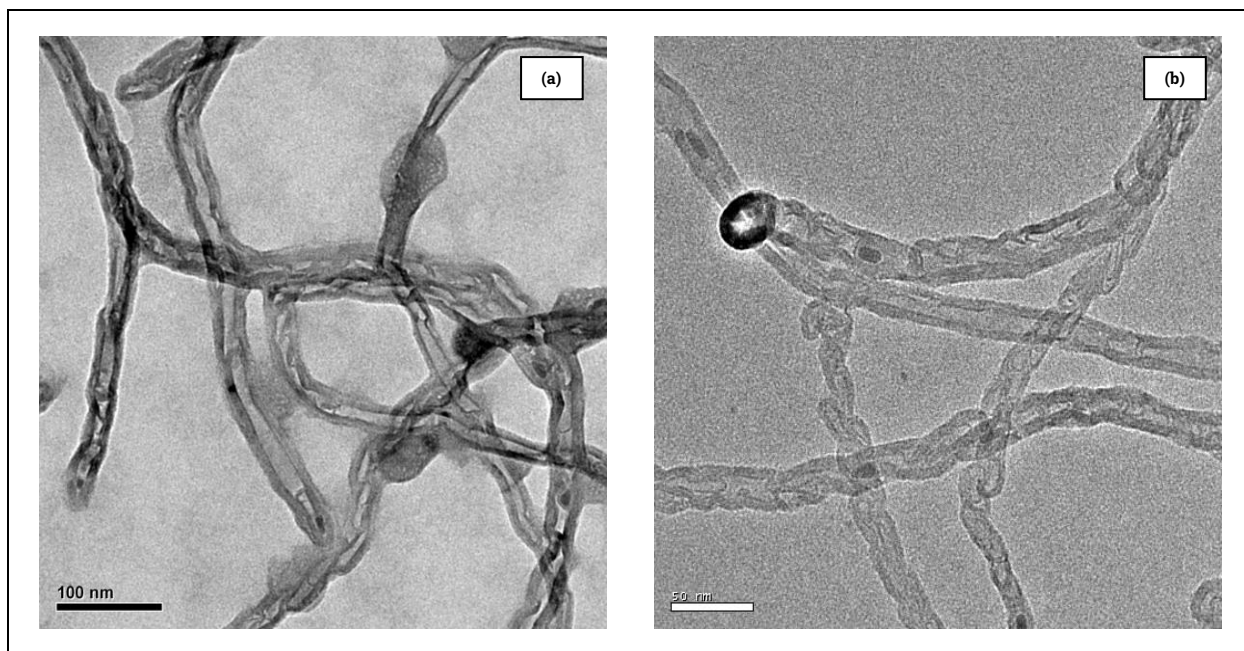

Fig. 8: HRTEM image of MWNTs with catalyst composition (a) 0.25 g (b) 0.50 g

3.3 Numerical Optimization

To find the best solution, response surfaces are engaged. Any combination of one or more goals can be optimized using numerical optimization. Table 4 shows the numerical optimization solution. Figures 9a and 9b show the HRTEM images and Raman spectrum under optimal conditions. The consistency in the diameter of

CNTs is dependent on the pyrolysis temperature of the carbon precursor and hydrocarbon-catalyst interaction. The D and G peaks can be found at 1345 cm⁻¹ and 1543 cm⁻¹, respectively. The lack of radial breathing modes at lower frequencies (RBM) showed the absence of single walled carbon nanotubes. The I_G/I_D proportion estimated from the peak region is 1.59.
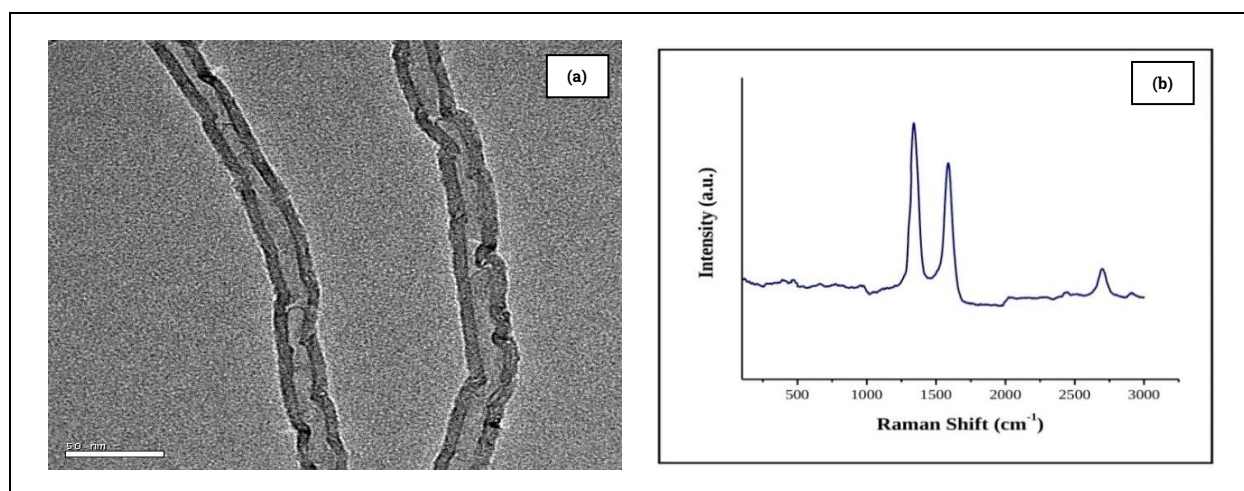

Fig. 9: a) HRTEM image and b) Raman Spectrum of MWNTs grown at optimum condition

Table 4. Most favorable values of the procedure variables and response

Variables	*Citrus limonum* oil
Temperature (°C)	671.31
Catalyst composition (g)	0.53
Precursor Feed rate (mL)	22.91
Yield percentage (Predicted)	79.30
Yield percentage (Actual)	79

3.4 Photocatalytic Degradation of Sudan Black B

3.4.1 Effect of initial dye concentration

A significant factor optimized was the effect of dye concentration (Fig. 10a). With an increase in starting H_2O_2 concentration, the amount of decolorization of Sudan black B dye increases to 300 mg. Decolorization then begins to decline. As a result, we conclude that 300 mg is the ideal concentration because it has the greatest amount of decolorization. This is due to: i) as the dye concentration increases, there is more dye substrate in the solution relative to a fixed number of •OH radicals, ii) the decrease in decolorization efficiency with an increase in the number of molecules to be oxidized under the same operating conditions, and iii) the intermediates may have consumed reactive free radicals, resulting in competitive parallel reactions between these free radicals and the intermediates and Sudan black dye.

3.4.2 Effect of H_2O_2

The proportion of hydrogen peroxide has a significant impact on Sudan black B degradation. By irradiating the dye solution with various H_2O_2 dosages, the effect of initial H_2O_2 concentration on dye decolorization was investigated (50-500 mM). The percentage of deterioration ranges from 62.27 to 69.62. (Fig 10 b). The use of oxidant is the most important factor influencing the cost of any Advanced Oxidation Process (AOP). As a result, optimizing the amount of oxidant used in any AOP is critical for cost-effective industrial wastewater treatment. In the study, the primary oxidant that produced free radicals was H_2O_2. The graph shows that increasing the concentration of H_2O_2 causes Sudan black B to decolorize to a concentration of 350 mM. Following that, the amount of decolorization decreased. Thus, 350 mM is the best concentration for decolorization, which is due to production of more hydroxyl radicals as the concentration of H_2O_2 increases, which can attack more dye molecules. When there is an excess of H_2O_2, the hydroxyl radicals act as scavengers, resulting in less dye decolorization (Padmavathi *et al.* 2022).

3.4.3 Effect of catalyst concentration

Figure 10c depicts the effect of photocatalyst concentration (50-500 mg/L) on Sudan black B 10 degradation (MWNTs grown on Fe-Co-Mo catalyst). To improve catalyst diffusion, the photocatalyst (Fe-Co-Mo catalyst-grown MWNTs) was added to the dye solution and thoroughly mixed. The previously mentioned solution was exposed to sunlight to degrade. The figure depicts the impact of catalyst concentration on dye degradation. The concentration of catalyst (CNT) varies from 50 mg/L to 300 mg/L. The decolorization decreases as the catalyst concentration (CNT) increases. As a result, we determined that the best catalyst concentration is 100 mg/L. Decolorization is reduced as catalyst concentration increases, resulting in a greater catalyst total active surface area, leading to the unavailability of dye molecules. Light penetration into the dye solution was reduced even after reaching the optimal level of catalyst concentration due to increased light scattering by the

catalyst's surface area (Sachin *et al*. 2020).

3.4.4 Effect of solar light intensity

Increased solar light intensity causes dye decolorization. It is because of the following factors:

i) the generation of photons increases as the intensity of solar radiation increases, ii) the photocatalyst absorbs more photons and generates more hydroxyl radicals (Fe-Co-Mo catalyst-grown MWNTs) (Fig. 10d) and iii) the dye molecules are attacked and degraded by a greater number of hydroxyl radicals (Suhila *et al*. 2020).
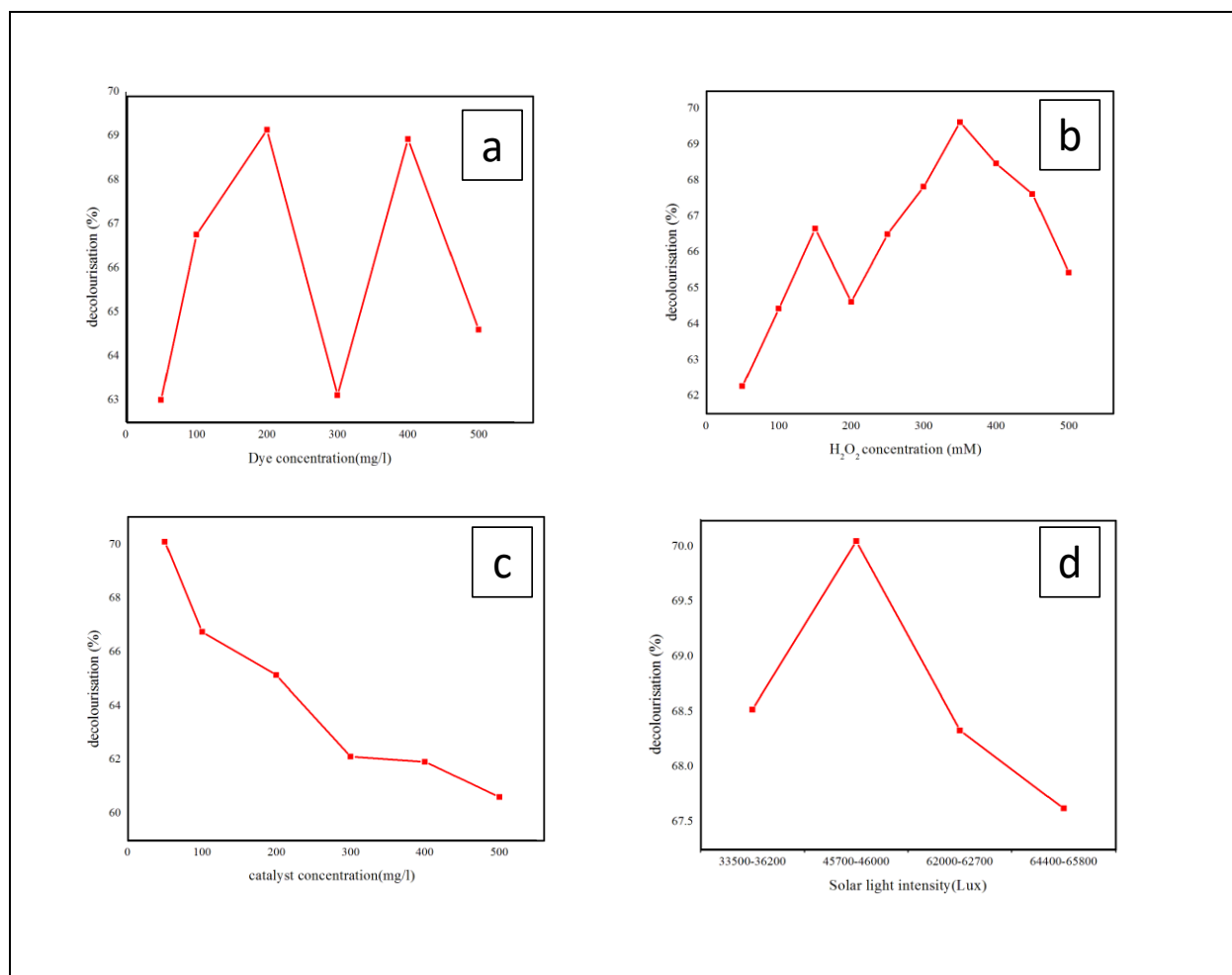

Fig. 10: a) Effect of initial dye concentration b) Effect of H$_2$O$_2$ c) Effect of catalyst concentration d) Effect of solar light intensity

3.4.5 Reusability of photocatalyst

In practical applications, the reusability of photocatalysts is a critical and deciding factor. Because they absorb high-energy photons, most photocatalytic materials corrode when exposed to light. After the dye degradation process, the used photocatalyst was separated and dehydrated in an oven for 30 minutes at 70°C. Figure 11 shows that after three cycles of reusability, only 13% of photocatalyst activity was reduced. This indicates that the photocatalyst synthesized has excellent stability, with minimal optical corrosion and photocatalyst activity loss. After three cycles of re-used photocatalyst, 70% of Sudan black B was degraded,

indicating that the nano photocatalyst is reusable, functional, and active in environmental applications (Ahmad *et al*. 2019).

3.4.6 Mechanism

Figure 12 depicts the dye degradation mechanism of Sudan black B. When dye molecules are exposed to sunlight, they become activated and shift electrons from the valence band to the conduction band. When an electron in the conduction band reduces molecular oxygen, a superoxide radical is generated (Padmavathi *et al*. 2021).
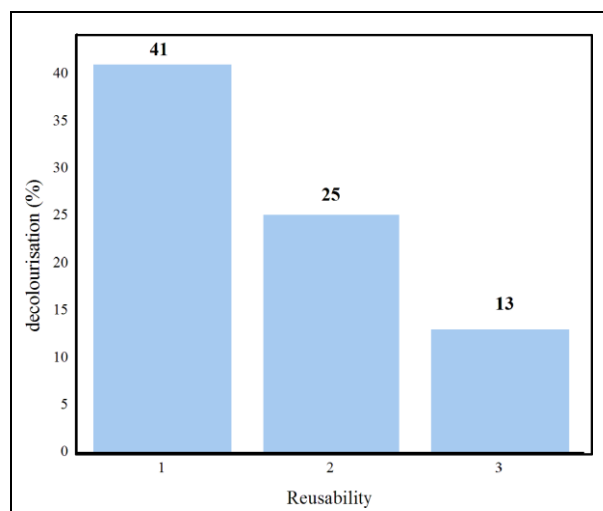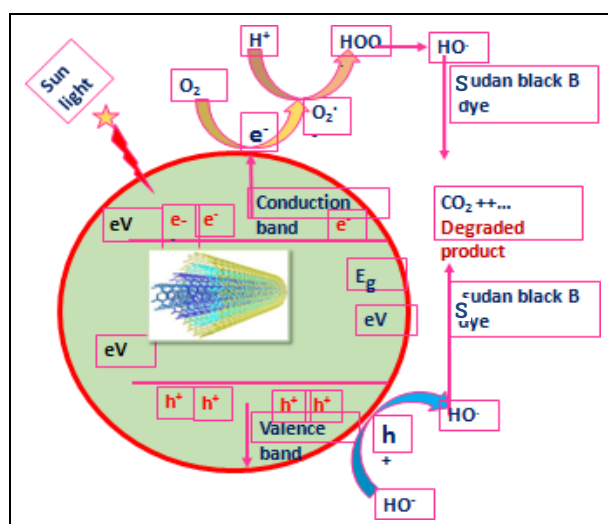
Fig. 11: Effect of reusability of photocatalyst

Fig. 12: Schematic diagram for degradation mechanism of Sudan black B dye

4. CONCLUSION

In order to maximize the production of MWCNTs synthesized utilizing *Citrus limonum* oil as the carbon precursor, a Box-Behnken design of experiment based on response surface approach was employed in this study. By using the ideal conditions, the highest yield of CNT was generated. This experiment suggests that the ideal conditions are: a reaction temperature of 671.31℃, a catalyst composition of 0.53 g, and precursor feed rate of 22.91 mL. This efficient method can be employed for maximizing CNT yield in large-scale industries. According to the results of the studies, the amount of decolorization of Sudan black B dye increases up to a certain level with an increase in starting H_2O_2 concentration and then decreases as excess hydroxyl radicals produced act as scavengers, resulting in reduced dye decolonization. It has also been found that the optimal catalyst concentration is 100 mg/L.

CONFLICTS OF INTEREST

The authors declare no competing interests.

DATA AVAILABILITY

The data generated or analyzed during this study is included in this published article.

AUTHOR CONTRIBUTION STATEMENT

Angulakshmi V. S. - Synthesis of CNTs and RSM modeling- major contributor in paper content.

Mageswari, S. - Executed preparation of catalyst nanoparticle and characterization.

Kalaiselvan, S. - Explication & investigation. Writing review, editing and supervision.

Padmavathi, R. - Effect of photo degradation studies on MWCNTs.

Parvathi, K. - Purification of CNTs and characterization. All the authors read and approved the final version of this manuscript.

REFERENCES

Aarthi, T., Narahari, P. and Madras G., Photocatalytic degradation of Azure and Sudan dyes using nano TiO2, *J. Hazard Mater.,* 149(3), 725-734 (2007). https://doi.org/10.1016/j.jhazmat.2007.04.038

Ahmad, N., Mohammad, H., Ebrahim, A. A. and Hamed, B., Sono-solvothermal design of nanostructured flowerlike BiOI photocatalyst over silica-aerogel with enhanced solar-light-driven property for degradation of organic dyes, *Sep. Purif. Technol.,* 221, 101–113 (2019). https://doi.org/10.1016/j.seppur.2019.03.075

Amirhasan, N., Bahram, G., Mostafa, Z. and Ezatollah, A., Morphology Optimization of CCVD-Synthesized multiwall carbon nanotubes, using statistical design of experiments, *Nanotechnol.,* 18 (11), 115715 (2007). https://doi.org/10.1088/0957-4484/18/11/115715

Aqel, AAbou, E. N. K. M. M., Ammar, R. A. A. and Warthan, A. A., Carbon nanotubes, science and technology part (I) structure, synthesis and characterization, *Arabian J. Chem.,* 5(1), 1–23 (2012). https://doi.org/10.1016/j.arabjc.2010.08.022

Arunachalam, S., Gupta, A. A., Izquierdo, R. and Nabki, F., Suspended Carbon Nanotubes for Humidity Sensing, *Sens.*, 18(5), 1-11 (2018). https://doi.org/10.3390/s18051655

César, R. T. T., Vivian, S. S., Bruno, E. L. B., Arnaldo, C. P. and Lauro, T. K., Simultaneous determination of zinc, cadmium and lead in environmental water samples by potentiometric stripping analysis (PSA) using multiwalled carbon nanotube electrode, *J. Hazard. Mater.,* 169(1–3), 256-262 (2009). https://doi.org/10.1016/j.jhazmat.2009.03.077

Chaudhary, D., Khare, N. and Vankar, V. D., Ag nanoparticles loaded TiO2/MWCNT ternary nanocomposite: a visible-light-driven photocatalyst with enhanced photocatalytic performance and stability, *Ceram. Int.,* 42 (14), 15861–15867 (2016). https://doi.org/10.1016/j.ceramint.2016.07.056

Chen, S., Shan, B., Yang, Y., Yuan, G., Huang, S., Lu, X., Zhang, Y., Fu, Y., Ye, L. and Liu, J., An overview of carbon nanotubes based interconnects for microelectronic packaging, *2017 IMAPS Nordic Conference on Microelectronics Packaging (NordPac), Gothenburg, Sweden,* 18–20, 113–119 (2017). https://doi.org/10.1109/NORDPAC.2017.7993175

Choi, J., Park, B. C., Ahn, S. J., Kim, D. H., Lyou, J., Dixson, R. G., Orji, N. G., Fu, J. and Vorburger, T. V., Evaluation of carbon nanotube probes in critical dimension atomic force microscopes, *J. Micro/Nanolithogr. MEMS MOEMS,* 15(3), 1-13 (2016). https://doi.org/10.1117/1.JMM.15.3.034005

Chua, M., Chui, C. K., Chng, C. B. and Lau, D., Carbon nanotube-based artificial tracheal prosthesis: Carbon nanocomposite implants for patient-specific ENT care, *IEEE Nanotechnol. Mag.,* 7(4), 27–31 (2013). https://doi.org/10.1109/MNANO.2013.2289691

Coville, N. J., Mhlanga, S. D., Nxumalo, E. N. and Shaikjee, A., A review of shaped carbon nanomaterials, *S. Afr. J. Sci.,* 107(3-4), 1–15 (2011). http://dx.doi.org/10.4102/sajs.v107i3/4.418

Donaldson, K., Aitken, R., Tran, L., Stone, V, Duffin, R., Forrest, G. and Alexander, A., Carbon nanotubes: A review of their properties in relation to pulmonary toxicology and workplace safety, *Toxicol. Sci.,* 92(1), 5–22 (2006). https://doi.org/10.1093/toxsci/kfj130

Ghosh. P., Soga. T., Rakesh. A. and Afre, J. T., Simplified synthesis of single-walled carbon nanotubes from a botanical hydrocarbon: Turpentine oil, *J. Alloys Compd.,* 462(1-2), 289-293 (2008). https://doi.org/10.1016/j.jallcom.2007.08.027

Goh, T. N., A Pragmatic approach to experimental design in industry, *J. Appl. Stat.,* 28(3) 391-398 (2001). https://doi.org/10.1080/02664760120034126

Gupta, N., Gupta, S. M. and Sharma, S. K., Carbon nanotubes: Synthesis, properties and engineering applications. *Carbon Lett.,* 29, 419–447 (2019). https://doi.org/10.1007/s42823-019-00068-2

Hayati, F., Isari, A. A., Anvaripour, B., Fattahi, M. and Kakavandi, B., Ultrasound-assisted photocatalytic degradation of sulfadiazine using MgO@CNT heterojunction composite: effective factors, pathway and biodegradability studies, *Chem. Eng. J.,* 381, 122636, (2020). https://doi.org/10.1016/j.cej.2019.122636

Journet, C., Maser, W., Bernier, P., Loiseau, A., De, L., Chapelle, M. L., Lefrant, S., Deniard, P., Lee, R. and Fischer, J. E., Large-scale production of single-walled carbon nanotubes by the electric-arc technique, *Nat.,* 388, 756–758 (1997). https://doi.org/10.1038/41972

Kalaiselvan, S., Balachandran, K., Karthikeyan, S. and Venckatesh, R., Botanical hydrocarbon sources based MWCNTs synthesized by spray pyrolysis method for DSSC applications, *Silicon,* 10(2), 211-217 (2018). https://doi.org/10.1007/s12633-016-9419-7

Karthikeyan, S., Kalaiselvan, S., Anitha, K., Shanthi, P. and Shabudeen, P. S., Morphology of entangled multiwalled carbon nanotubes by catalytic spray pyrolysis using madhuca longifolia oil as a precursor, *Rasayan J. Chem.*, 7(4), 333-339 (2014).

Ketabi, S. and Rahmani, L., Carbon nanotube as a carrier in drug delivery system for carnosine dipeptide: A computer simulation study, *Mater. Sci. Eng C.,* 73, 173–181 (2017). https://doi.org/10.1016/j.msec.2016.12.058

Kumar, M. and Ando, Y., Controlling the diameter distribution of carbon nanotubes grown from camphor on a zeolite support, *Carbon,* 43(3), 533-540 (2005). https://doi.org/10.1016/j.carbon.2004.10.014

Kumar, S., Nehra, M., Kedia, D., Dilbaghi, N., Tankeshwar, K. and Kim, K. H., Carbon nanotubes: A potential material for energy conversion and storage, *Prog. Energy Combust. Sci.*, 64, 219–253 (2018).
https://doi.org/10.1016/j.pecs.2017.10.005

Kumar. M., Okazaki, T., Hiramatsu, M. and Ando, Y., The use of camphor-grown carbon nanotube array as an efficient field emitter, *Carbon,* 45(9), 1899-1904 (2007).
https://doi.org/10.1016/j.carbon.2007.04.023

Lee, J., Kim, T., Jung, Y., Jung, K., Park, J., Lee, D. M., Jeong, H. S., Hwang, J. Y., Park, C. R. and Lee, K. H., High-strength carbon nanotube/carbon composite fibers via chemical vapor infiltration, *Nanoscale,* 8, 18972–18979 (2016).
https://doi.org/10.1039/C6NR06479E

Li, W. Z., Wen, J. G. and Ren, Z. F., Effect of temperature on growth and structure of carbon nanotubes by chemical vapor deposition, *Appl.Phys. A,* 74, 397-402 (2002).
https://doi.org/10.1007/s003390201284

Mageswari. S., Kalaiselvan. S., Shabudeen, P. S. S., Sivakumar. N. and Karthikeyan, S., Optimization of growth temperature of multi-walled carbon nanotubes fabricated by chemical vapour deposition and their application for arsenic removal, *Mater. Sci. Poland*, 32(4), 709-718 (2014).
https://doi.org/10.2478/s13536-014-0235-8

Moise, C., Rachmani, L., Mihai, G., Lazar, O., Enăchescu, M. and Naveh, N., Pulsed laser deposition of SWCNTs on carbon fibres: Effect of deposition temperature, *Polym.,* 13(7), 1-13 (2021).
https://doi.org/10.3390/polym13071138

Othman, C. S., Al, H., Isaiah, O. A. and Tawfik, A. S., Novel cross-linked melamine based polyamine/CNT composites for lead ions removal, *J. Environ. Manage.*, 192, 163-170 (2017).
https://doi.org/10.1016/j.jenvman.2017.01.056

Padmavathi, R. Raja, R., Kalaivanan, C. and Kalaiselvan, S., Syzygium Cumini leaf extract exploited in the green synthesis of zinc oxide nanoparticles for dye degradation and antimicrobial studies, *Mater. Today Proc.*, 69(3), 1200-1205 (2022).
https://doi.org/10.1016/j.matpr.2022.08.257

Padmavathi, R., Sharmil, L. I., Prasad, S., Thamarai, S. M. and Kalaiselvan, S., Utilization of solar energy for photodegradation of basic violet 10 using tin oxide doped ZnO, *J. Ovonic Res.,* 17(3), 261-271 (2021).
https://doi.org/10.15251/jor.2021.173.261

Piedigrosso, P., Knoya, Z., Colomer, J. F., Fonseca, A., Tendeloo, G. V. and Nagy, J. B., Production of differently shaped multiwall carbon nanotubes using various cobalt supported catalysts, *PCCP,* 2(1), 163-170 (2000).
https://doi.org/10.1039/A905622J

Rakesh, A. A., Soga, T., Jimbo, T., Mukulkumar, Ando, Y., Sharon, M., Prakash, R. S. and Umeno, M., Carbon nanotubes by spray pyrolysis of turpentine oil at different temperatures and their studies, *Microporous Mesoporous Mater.,* 96, 1-3, 184-190 (2006).
https://doi.org/10.1016/j.micromeso.2006.06.036

Sachin, G. S., Maheshkumar, P. P., Gun, D. K. and Vinod, S. S., Ni, C, N, S multi-doped ZrO2 decorated on multi-walled carbon nanotubes for effective solar induced degradation of anionic dye, *J. Environ. Chem. Eng.,* 8(3), 103769 (2020).
https://doi.org/10.1016/j.jece.2020.103769

Sankeerthana, B., Nithya, T., Hafeez, Y. H., Neppolian, B. and Ranga, R. G., Highly active and stable multi-walled carbon nanotubes-graphene-TiO2 nanohybrid: An efficient non-noble metal photocatalyst for water splitting, *Catal. Today,* 321, 120-127 (2019).
https://doi.org/10.1016/j.cattod.2017.10.023

Shaban, M., Ashraf, A. M., Mostafa, R. A., TiO2 Nanoribbons/Carbon nanotubes composite with enhanced photocatalytic activity; fabrication, characterization and application, *Sci. Rep.,* 8, 1-17 (2018).
https://doi.org/10.1038/s41598-018-19172-w

Suhila, A., Aïcha, M., Elbashir, E., Ali, S., Photocatalytic degradation of methylene blue dye in aqueous solution by $MnTiO_3$ nanoparticles under sunlight irradiation, Heliyon, 6(4), e03663 (2020).
https://doi.org/10.1016/j.heliyon.2020.e03663

Sun, Y., Yun, K. N., Leti, G., Lee, S. H., Song, Y. H. and Lee, C. J., High-performance field emission of carbon nanotube paste emitters fabricated using graphite nanopowder filler, *Nanotechnol.,* 28(6), 065201 (2017).
https://doi.org/10.1088/1361-6528/aa523e

Uthayakumar, H., Radhakrishnan, P., Shanmugam, K. and Kushwaha, O. S., Growth of MWCNTs from Azadirachta indica oil for optimization of chromium(VI) removal efficiency using machine learning approach, *Environ. Sci. Pollut. Res. Int.,* 29, 34841-34860 (2022).
https://doi.org/10.1007/s11356-021-17873-w

Wei, W. L., Azizan, A., Siang, P. C., Abdul, R. M. and Ching, T. T., Optimization of reaction conditions for the synthesis of single-walled carbon nanotubes using response surface methodology, *Can. J. Chem. Eng.,* 90(2), 489-505 (2012).
https://doi.org/10.1155/2013/592464

Willems, I., Konya, Z., Colomer, J. F., Tendeloo, G. V., Nagaraju, N., Fonseca, A. and Nagy, J. B., Control of the outer diameter of thin carbon nanotubes synthesized by catalytic decomposition of hydrocarbons, *AIP Conf. Proc.,* 544, 242-245 (2000). https://doi.org/10.1063/1.1342509

Xu, J. L., Dai, R. X., Xin, Y., Sun, Y. L., Li, X., Yu, Y. X., Xiang, L., Xie, D., Wang, S. D. and Ren, T. L., Efficient and reversible electron doping of semiconductor-enriched single-walled carbon nanotubes by using deca methylcobaltocene. *Sci. Rep.,* 7, 6751 (2017). https://doi.org/10.1038/s41598-017-05967-w

Yanase, T., Miura, T., Shiratori, T., Weng, M., Nagahama, T. and Shimada, T., Synthesis of carbon nanotubes by plasma-enhanced chemical vapor deposition using Fe1−xMnxO nanoparticles as catalysts: How does the catalytic activity of graphitization affect the yields and morphology?, *Carbon,* 5(3), 46 (2019). https://doi.org/10.3390/c5030046

Zhao, T., Ji, X., Jin, W., Yang, W. and Li, T., Hydrogen storage capacity of single-walled carbon nanotube prepared by a modified arc discharge, *Fuller. Nanotubes Carbon Nanostruct.*, 25(6), 355–358 (2017). http://dx.doi.org/10.1080/1536383X.2017.1305358